Constructing “chaotic coordinates” for non-integrable dynamical systems

S. R. Hudson, Princeton Plasma Physics Laboratory

Abstract

Action-angle coordinates can be constructed for so-called integrable Hamiltonian dynamical systems, for which there exists a foliation of phase space by surfaces that are invariant under the dynamical flow.

Perturbations generally destroy integrability.

However, we know that periodic orbits will survive, as will cantori, as will the “KAM” surfaces that have sufficiently irrational frequency, depending on the perturbation. There will also be irregular “chaotic” trajectories.

By “fitting” the coordinates to the invariant structures that are robust to perturbation, action-angle coordinates may be generalized to non-integrable dynamical systems. These coordinates “capture” the invariant dynamics and neatly partition the chaotic regions. These so-called chaotic coordinates are based on a construction of almost-invariant surfaces known as ghost surfaces. The theoretical definition and numerical construction of ghost surfaces and chaotic coordinates will be described and illustrated.

Ghost Surfaces: theoretical definition

Classical Mechanics 101:

The action integral is a functional of a curve in phase space.

1. The action, S, is the line integral along an arbitrary "trial" curve $\{\mathcal{C} : q \equiv q(t)\}$, of the Lagrangian,

$$\mathcal{L} \equiv \underbrace{T(\dot{q}, q)}_{\text{kinetic}} - \underbrace{U(q,t)}_{\text{potential}}, \quad S \equiv \int_{\mathcal{C}} \mathcal{L}(q, \dot{q}, t) dt$$

2. For magnetic fields, $\mathbf{B}$, the action is the line integral, of the vector potential, $\mathbf{B} = \nabla \times \mathbf{A}$,

$$S \equiv \int_{\mathcal{C}} \mathbf{A} \cdot d\mathbf{l}, \text{ along } \{\mathcal{C} : \theta \equiv \theta(\zeta), \rho \equiv \rho(\theta)\}. \qquad \int \mathbf{A} \cdot d\mathbf{l} = \int \mathbf{B} \cdot d\mathbf{s} = \text{flux}$$

3. Physical trajectories (magnetic fieldlines) extremize the action:

$$\delta S = \int_{\mathcal{C}} d\zeta \left(\delta\theta \frac{\partial S}{\partial \theta} + \delta\rho \frac{\partial S}{\partial \rho} \right), \text{ where } \boxed{\frac{\partial S}{\partial \theta} \equiv \sqrt{g} B^{\rho} - \dot{\rho} \sqrt{g} B^{\zeta}} \text{ and } \boxed{\frac{\partial S}{\partial \rho} \equiv \dot{\theta} \sqrt{g} B^{\zeta} - \sqrt{g} B^{\theta}}.$$

extremal curves satisfy $\dot{\rho} = B^{\rho}/B^{\zeta}$, and $\dot{\theta} = B^{\theta}/B^{\zeta}$.

4. Action-extremizing periodic curves may be minimizing or minimax.

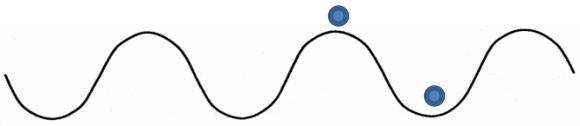

5. [Ghost surfaces are defined by an action-gradient flow between the minimax and minimizing periodic orbit.]

1954 : Kolmogorov, Dokl. Akad. Nauk SSSR 98, 469 ,1954

1963 : Arnold, Russ. Math. Surveys 18, 9,1963

1962 : Moser, Nachr. Akad. Wiss. Goett. II, Math.-Phys. Kl. 1, 1,1962

1. A dynamical system is integrable if there exists action-angle (ψ, θ) s.t. $H = H_0(\psi)$.

2. Arbitrary perturbation $H = H_0(\psi) + \sum_{m,n} H_{m,n}(\psi) \exp[i(m\theta - n\zeta)]$, where $\zeta \equiv t$ is "time".

3. Generating function to new action-action coordinates, $(\bar{\psi}, \bar{\theta})$, is

$$S(\bar{\psi}, \bar{\theta}) = \bar{\psi} \cdot \bar{\theta} + i \sum \frac{H_{m,n}}{(m\,\dot{\theta} - n)} \exp[i(m\theta - n\zeta)]. \qquad (1)$$

   i. small denominators: rationals are dense; $\exists (m, n)$ s.t. $m\,\dot{\theta} - n$ is arbitrarily small.

4. KAM: adjust ψ, iteratively, to ensure that $\iota \equiv \dot{\theta}$ is sufficiently irrational,

Diophantine condition $\boxed{\left|\iota - \frac{n}{m}\right| > \frac{r}{m^k}}$, for all n & m, where $r \geq 0$ and $k > 1$.

5. If ι is sufficiently irrational then for sufficiently small $H_{m,n}(\psi)$, Eqn(1) converges.

   i. action-angle coordinates can be constructed locally if $\iota \equiv \dot{\theta}$ is irrational.

"one of the most important concepts is labelling orbits by their frequency" [J. D. Meiss, Reviews of Modern Physics, 64(3):795 (1992)]

The structure of phase space is related to the structure of rationals and irrationals.

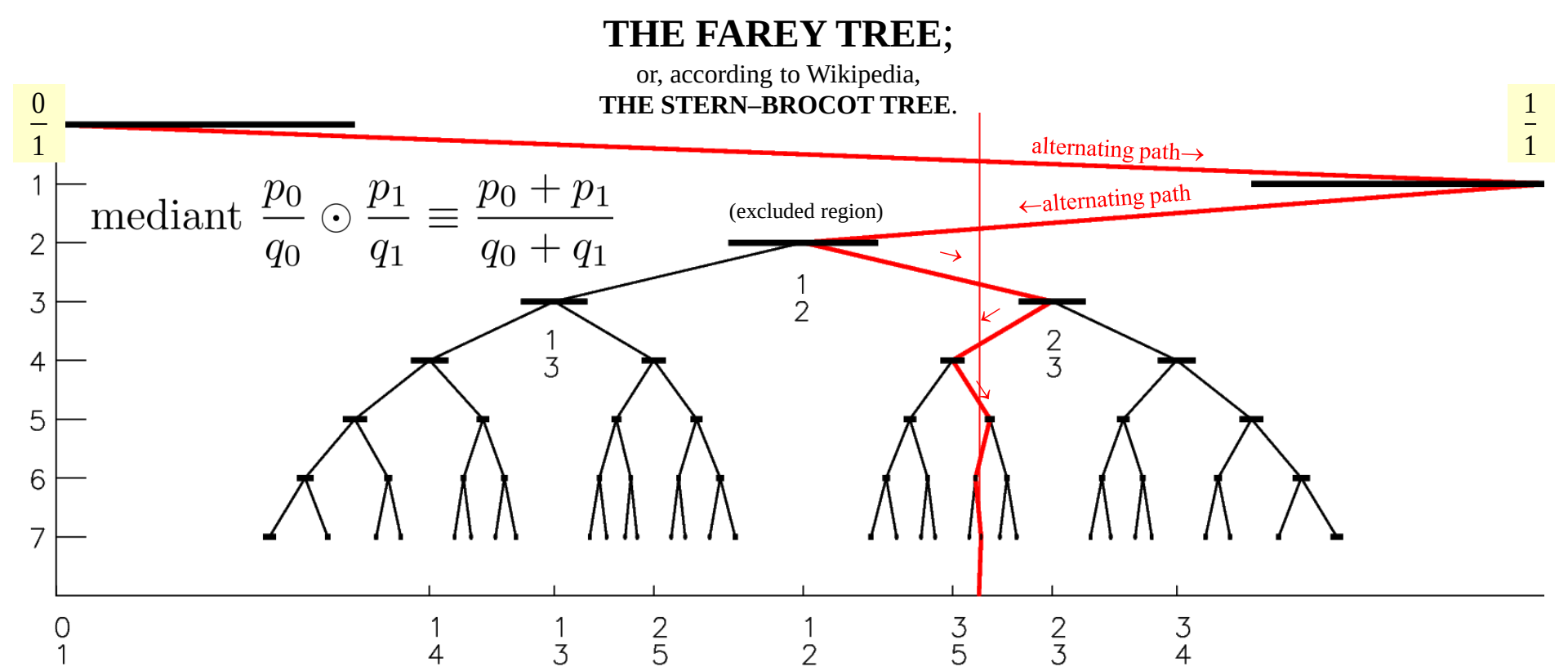

1. Islands, and chaos, emerge at every rational.

2. Noble irrationals ≡ limit of ultimately alternating paths ≡ limit of Fibonacci ratios

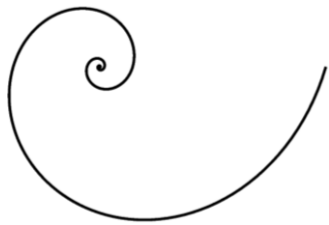

Irrational KAM surfaces break into cantori when perturbation exceeds critical value.
Both KAM surfaces and cantori restrict transport.

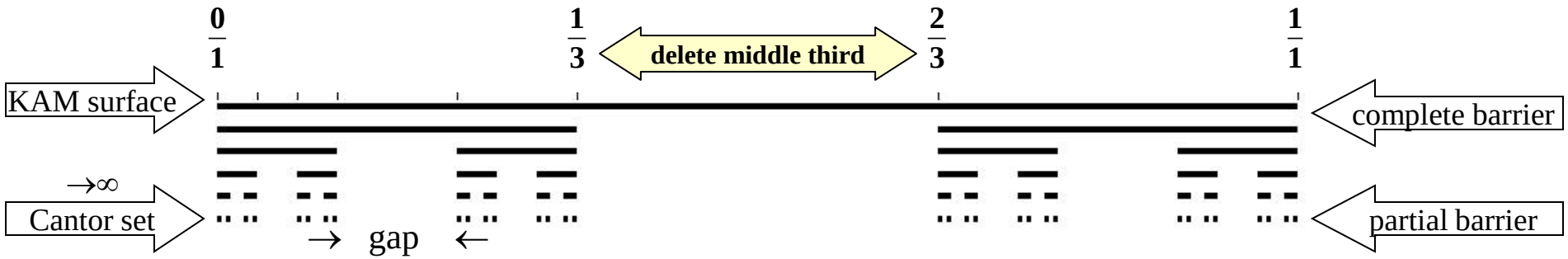

→ KAM surfaces are closed, toroidal surfaces that **stop** radial field line transport

→ Cantori have "gaps" that fieldlines can pass through; however, **cantori can severely restrict** radial transport

→ Example: all flux surfaces destroyed by chaos, but even after **100 000 transits** around torus the fieldlines **don't get past cantori !**

→ Regions of chaotic fields can provide some confinement because of the cantori partial barriers.

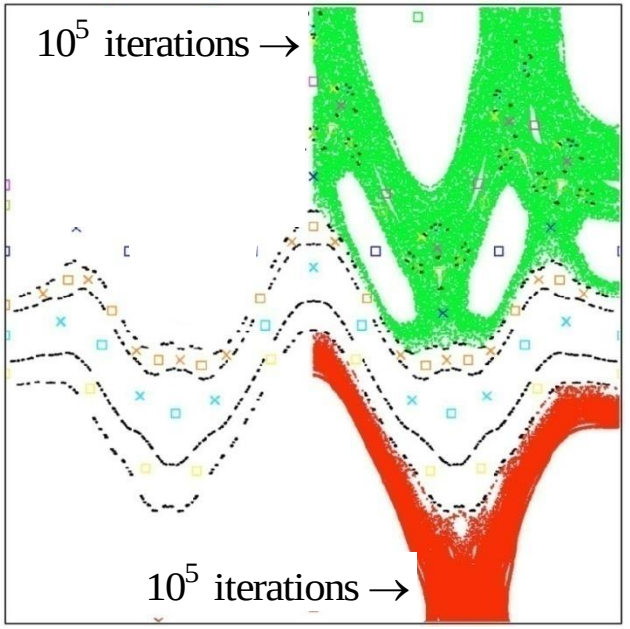

Simple physical picture of cantori

[Percival, 1979]

1. Consider masses, m, linked by springs in a periodic potential.

2. For $m = 0$, potential is irrelevant: minimum energy state has masses equally spaced.

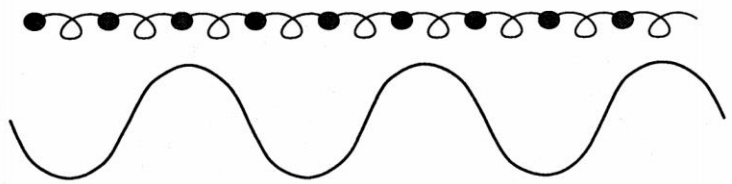

3. For large m, springs are irrelvant: all the masses lie at the potential minimum, and there are "gaps".

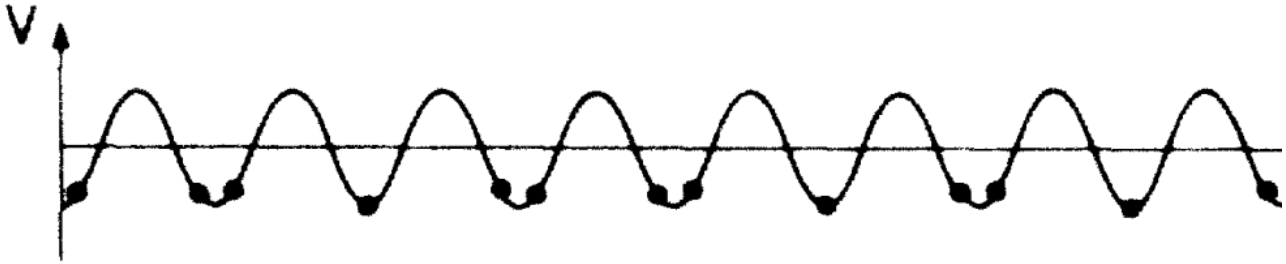

[Schellnhuber, Urbschat & Block, Physical Review A, 33(4):2856 (1986)]

The construction of extremizing curves of the action
generalized extremizing surfaces of the quadratic-flux

1. $\delta S = \int_{\mathcal{C}} d\zeta \left(\delta\theta \frac{\partial S}{\partial \theta} + \delta\rho \frac{\partial S}{\partial \rho} \right)$, where $\boxed{\frac{\partial S}{\partial \theta} \equiv \sqrt{g} B^{\rho} - \dot{\rho} \sqrt{g} B^{\zeta}}$ and $\boxed{\frac{\partial S}{\partial \rho} \equiv \dot{\theta} \sqrt{g} B^{\zeta} - \sqrt{g} B^{\theta}}$.

2. Extremal curves satisfy $\frac{\partial S}{\partial \theta} = 0$, i.e. $\dot{\rho} = B^{\rho}/B^{\zeta}$, and $\frac{\partial S}{\partial \rho} = 0$, i.e. $\dot{\theta} = B^{\theta}/B^{\zeta}$.

3. Introduce toroidal surface, $\rho \equiv P(\theta, \zeta)$, and *family* of angle curves, $\theta_{\alpha}(\zeta) \equiv \alpha + p\,\zeta/q + \tilde{\theta}(\zeta)$, where α is a fieldline label; p and q are integers that determine periodicity; and $\tilde{\theta}(0) = \tilde{\theta}(2\pi q) = 0$.

4. On *each* curve, $\rho_{\alpha}(\zeta) = P(\theta_{\alpha}(\zeta), \zeta)$ and $\theta_{\alpha}(\zeta)$, can <u>enforce</u> $\frac{\partial S}{\partial \rho} = 0$; generally $\nu \equiv \frac{\partial S}{\partial \theta} \neq 0$.

5. The *pseudo* surface dynamics is defined by $\dot{\theta} \equiv B^{\theta}/B^{\zeta}$ and $\dot{\rho} \equiv \partial_{\theta} P\, \dot{\theta} + \partial_{\zeta} P$.

6. Corresponding *pseudo* field $\mathbf{B}_{\nu} \equiv \dot{\rho}\, B^{\zeta}\, \mathbf{e}_{\rho} + \dot{\theta}\, B^{\zeta}\, \mathbf{e}_{\theta} + B^{\zeta} \mathbf{e}_{\zeta}$; simplifies to $\mathbf{B}_{\nu} = \mathbf{B} - \frac{\nu}{\sqrt{g}}\, \mathbf{e}_{\rho}$.

7. Introduce the **<u>quadratic-flux functional</u>**: $\boxed{\varphi_2 \equiv \frac{1}{2} \iint d\theta d\zeta \left(\frac{\partial S}{\partial \theta} \right)^2}$

8. Allowing for δP, the first variation is $\delta\varphi_2 = \iint d\theta d\zeta\, \delta P\, \sqrt{g}\, \underbrace{\left(B^{\theta} \partial_{\theta} + B^{\zeta} \partial_{\zeta} \right) \nu}_{\text{Euler-Lagrange for QFMs}}$.

At each poloidal angle, compute radial "error" field that must be subtracted from **B** to create a periodic curve, and so create a rational, pseudo flux surface.

0. Usually, there are only the "stable" periodic fieldline and the unstable periodic fieldline,

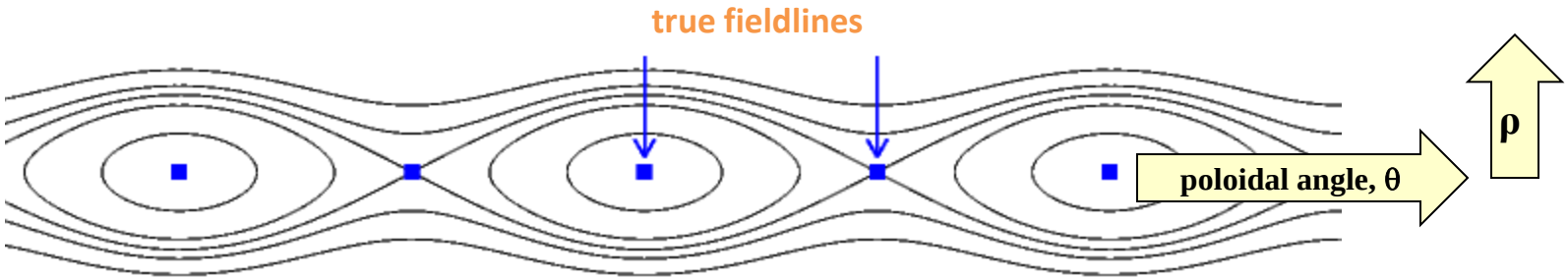

1. At every $\theta = \alpha$, determine $\nu(\alpha)$ via numerical search so that $\mathbf{B} - \nu\, \mathbf{e}_\rho/\sqrt{g}$ yields a periodic integral curve; where α is a fieldline label.

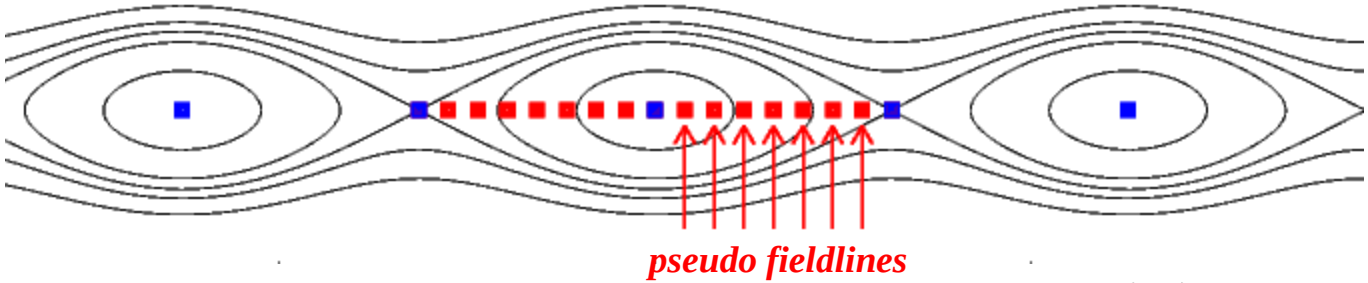

2. At the true periodic fieldlines, the required additional radial field is zero: i.e. $\nu(\alpha_0) = 0$ and $\nu(\alpha_X) = 0$.

3. Typically, $\nu(\alpha) \approx \sin(q\alpha)$.

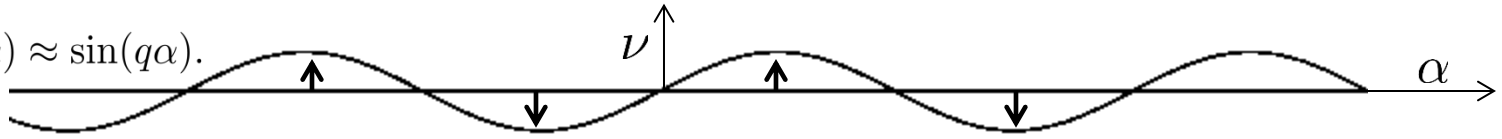

4. The pseudo fieldlines "capture" the true fieldlines; QFM surfaces pass through the islands.

Ghost surfaces, another class of almost-invariant surface, are defined by an action-gradient flow between the action minimax and minimizing fieldline.

1. Action, $S[\mathcal{C}] \equiv \int_{\mathcal{C}} \mathbf{A} \cdot d\mathbf{l}$, and action gradient, $\dfrac{\partial S}{\partial \theta} \equiv \sqrt{g} B^{\rho} - \dot{\rho} B^{\zeta}$.

2. Enforce $\dfrac{\partial S}{\partial \rho} \equiv \dot{\theta} B^{\zeta} - \sqrt{g} B^{\theta} = 0$, i.e. invert $\dot{\theta} \equiv B^{\theta}/B^{\zeta}$ to obtain $\rho = \rho(\dot{\theta}, \theta, \zeta)$; so that trial curve is completely described by $\theta(\zeta)$, and the action reduces from $S \equiv S[\rho(\zeta), \theta(\zeta)]$ to $S \equiv S[\theta(\zeta)]$

3. Define action-gradient flow: $\boxed{\dfrac{\partial \theta(\zeta;\tau)}{\partial \tau} \equiv -\dfrac{\partial S[\theta]}{\partial \theta}}$, where τ is an arbitrary integration parameter.

4. Ghost-surfaces are constructed as follows:

   i. Begin at action-minimax ("O", "not-always-stable") periodic fieldline, which is a saddle;
   ii. initialize integration in decreasing direction (given by negative eigenvalue/vector of Hessian);
   iii. the entire curve "flows" down the action gradient, $\partial_{\tau}\theta = -\partial_{\theta} S$;
   iv. action is decreasing, $\partial_{\tau} S < 0$;
   v. finish at action-minimizing ("X", unstable) periodic fieldline.
   vi. ghost surface described by $\mathbf{x}(\zeta, \tau)$, where τ is a fieldline label.

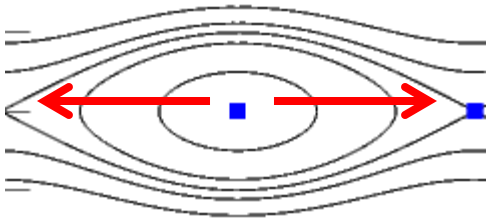

Ghost surfaces are (almost) indistinguishable from QFM surfaces

can redefine poloidal angle to unify ghost surfaces with QFMs.

1. Ghost-surfaces are defined by an (action gradient) flow.
2. QFM surfaces are defined by minimizing $\int (\text{action gradient})^2 d\mathbf{s}$.
3. Not obvious if the different definitions give the same surfaces.
4. For model chaotic field:
   (a) ghosts = thin solid lines;
   (b) QFMs = thick dashed lines;
   (c) agreement is excellent;
   (d) difference $= \mathcal{O}(\epsilon^2)$, where ϵ is perturbation.
5. Can redefine θ to obtain unified theory of ghosts & QFMs; straight *pseudo* fieldline angle.

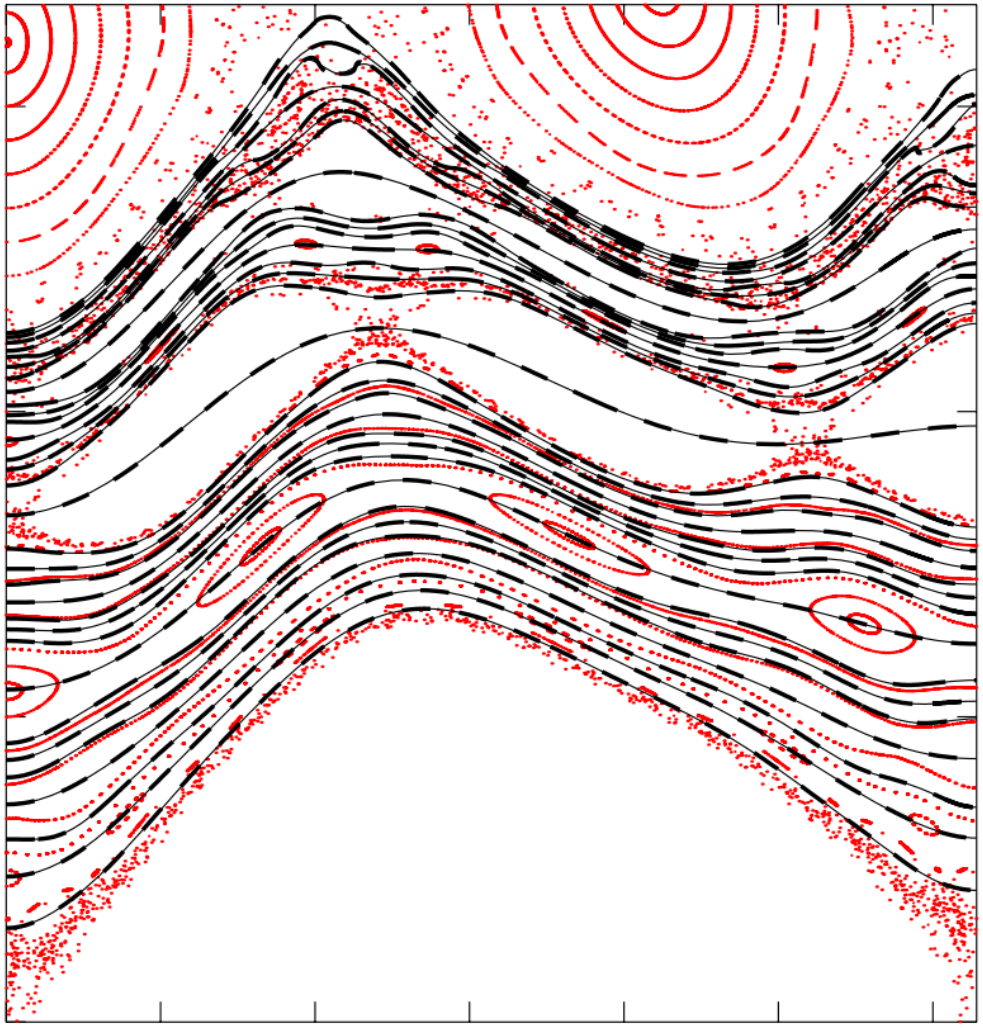

Chaotic Coordinates: intuitive description

Simplied Diagram showing the invariant structures: integrable

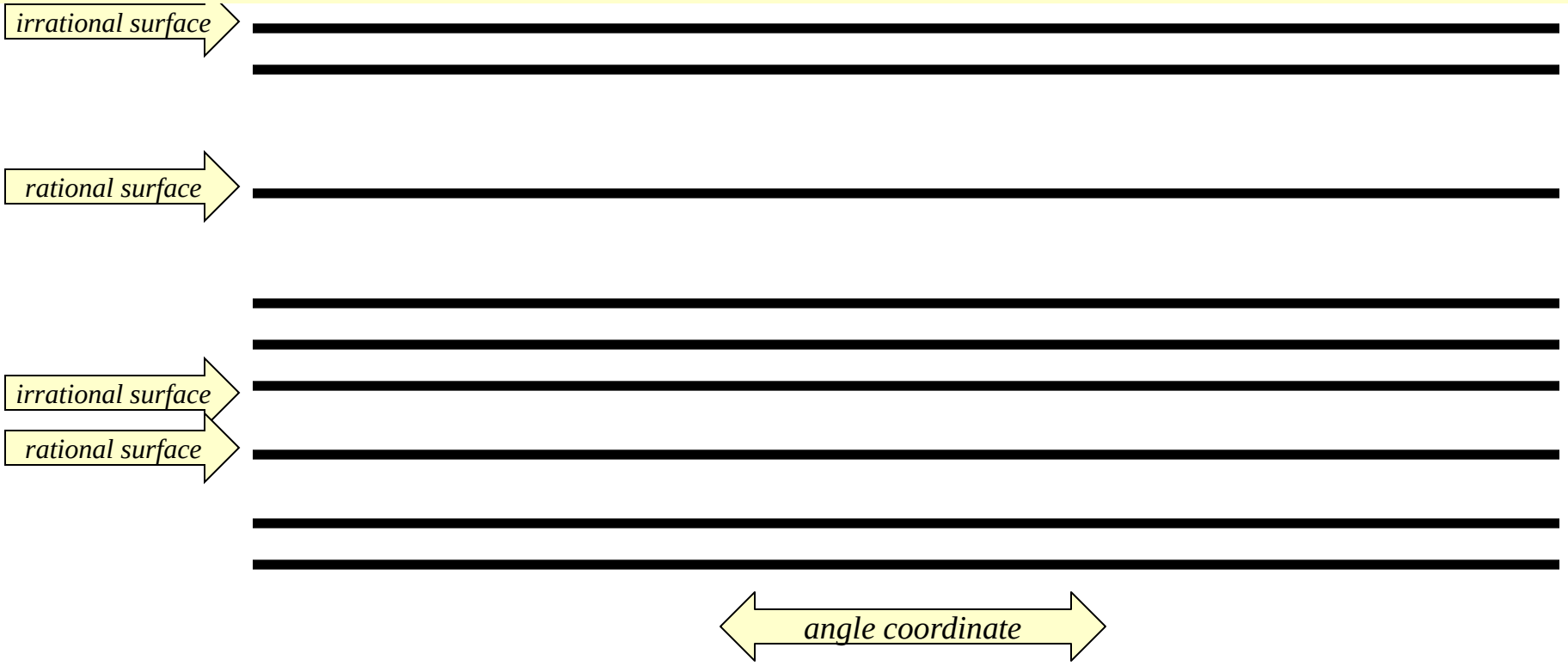

Action-angle coordinates can be constructed for "integrable" fields

1. the "action" coordinate coincides with the invariant surfaces
2. dynamics then appears simple

Simplied Diagram showing the invariant structures: perturbed

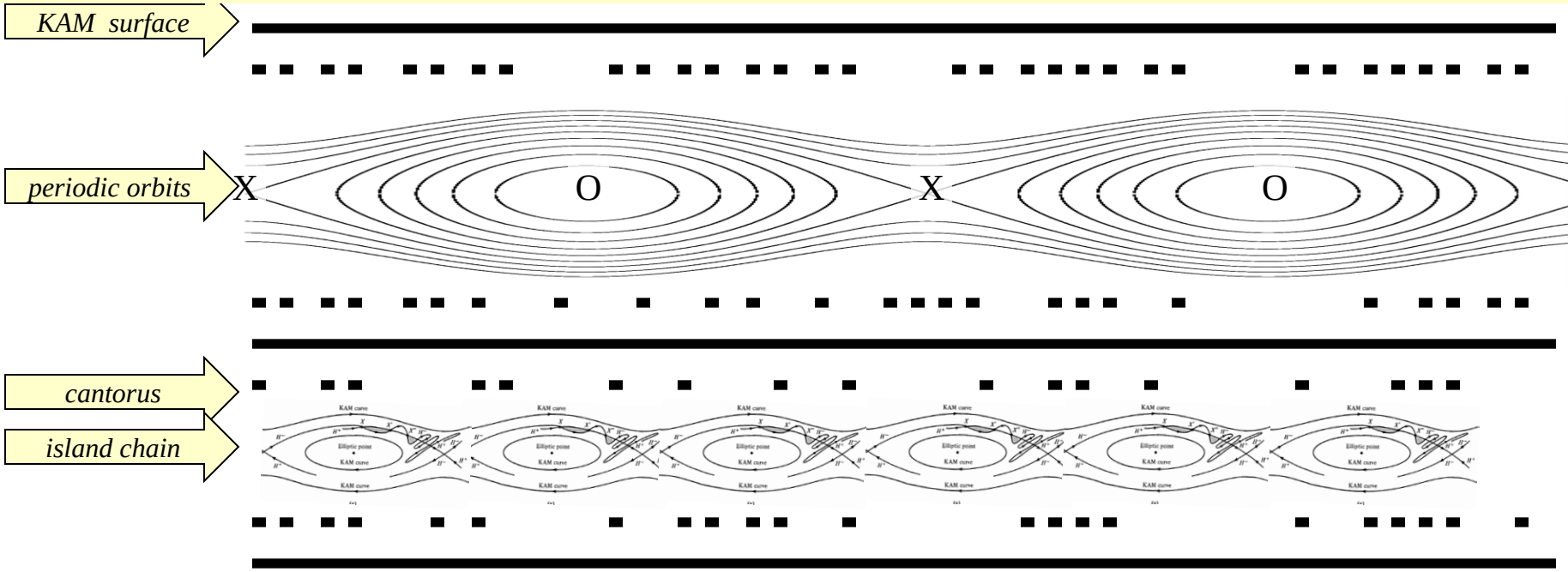

After perturbation:

the <u>rational</u> surfaces break into islands, “stable” and “unstable” periodic orbits survive,

some <u>irrational</u> surfaces break into cantori,

some <u>irrational</u> surfaces survive (KAM surfaces), break into cantori as perturbation increases,

→ action-angle coordinates can no longer be constructed globally

Simplied Diagram showing the invariant structures: perturbed

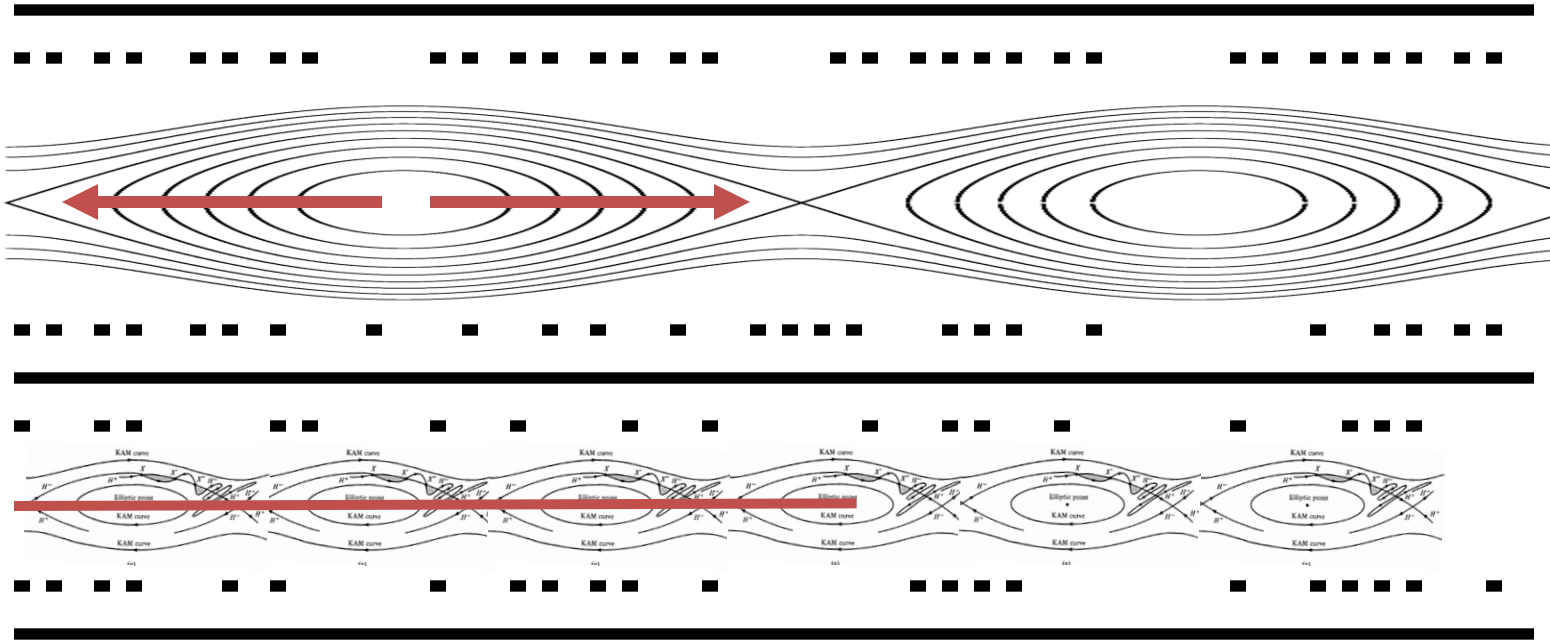

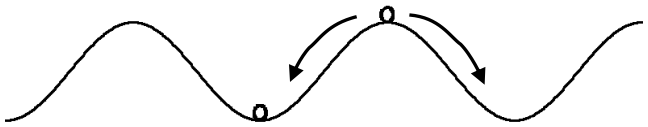

Simplied Diagram showing the invariant structures: perturbed, but with coordinates adapted to invariant sets

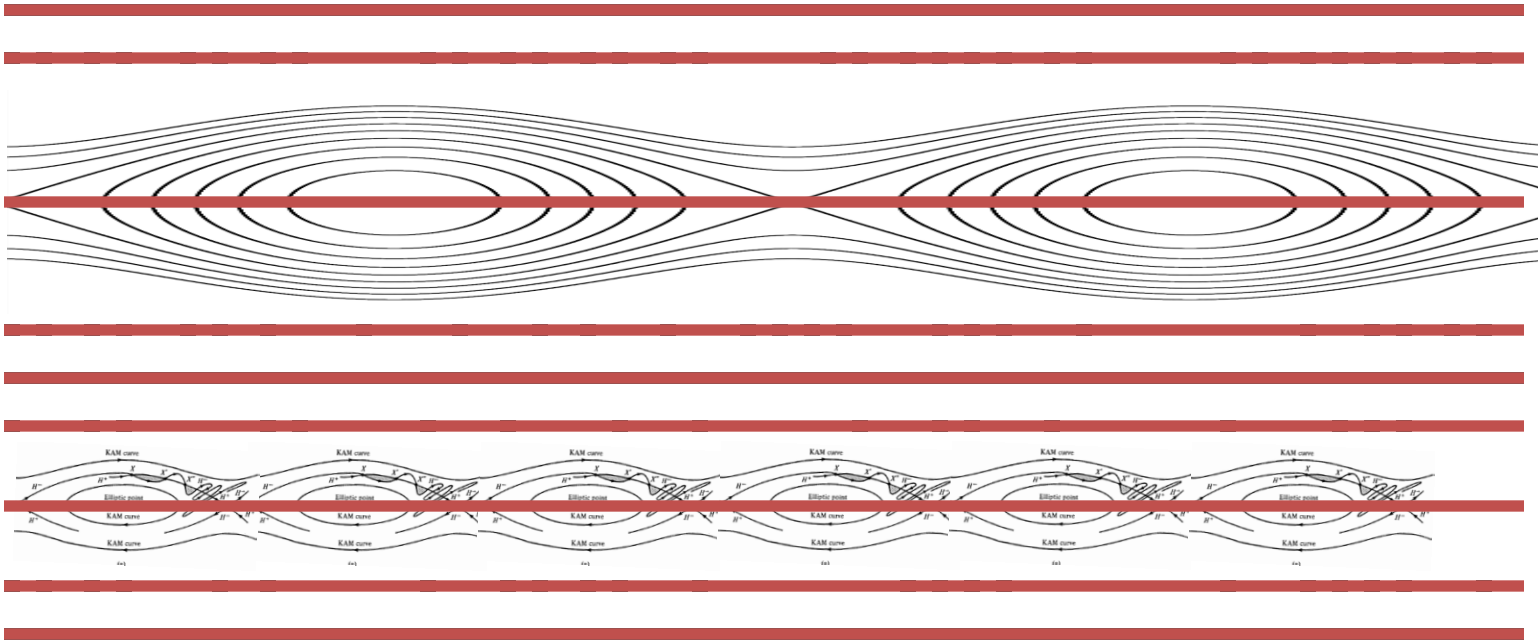

“Chaotic-coordinates” coincide with the invariant sets

1. coordinate surfaces are adapted to fractal hierarchy of remaining invariant sets
2. ghost surfaces ≡ quadratic-flux minimizing surfaces are “almost-invariant”
3. dynamics appears “almost-simple”

Simplied Diagram showing the invariant structures: example

Poincaré plot of chaotic field
(in **action-angle** coordinates of **unperturbed** field)

Poincaré plot of chaotic field
in chaotic coordinates

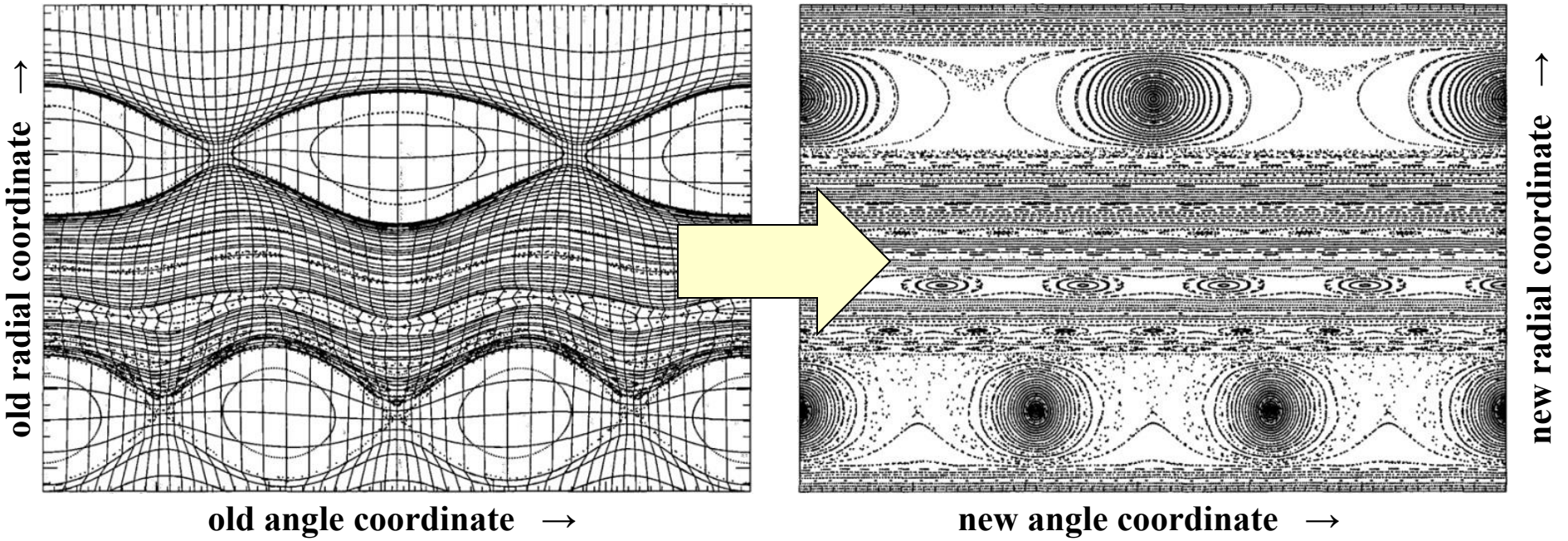

phase-space is partitioned into (1) regular “irrational” regions
and (2) irregular “rational” regions

Chaotic Coordinates: construction for stellarator fields

Large Helical Device (LHD) is a stellarator in Japan

1. The magnetic field consistent with an MHD equilibrium,
   $\nabla p \approx \mathbf{j} \times \mathbf{B}, \qquad \mathbf{j} \equiv \nabla \times \mathbf{B}$
   is provided by the HINT-2 code.

2. The field near the edge is chaotic.

3. A selection of ghost surfaces is constructed,
   $p/q = 10/23, 10/22, 10/21, \ldots$ near the axis,
   $p/q = 10/9, 10/8, 10/7, 10/6$ near the edge.
   (shown in lower half of figure)

4. These ghost surfaces, and a suitable interpolation provide a new coordinate system.

5. The following slides shall concentrate on edge region.

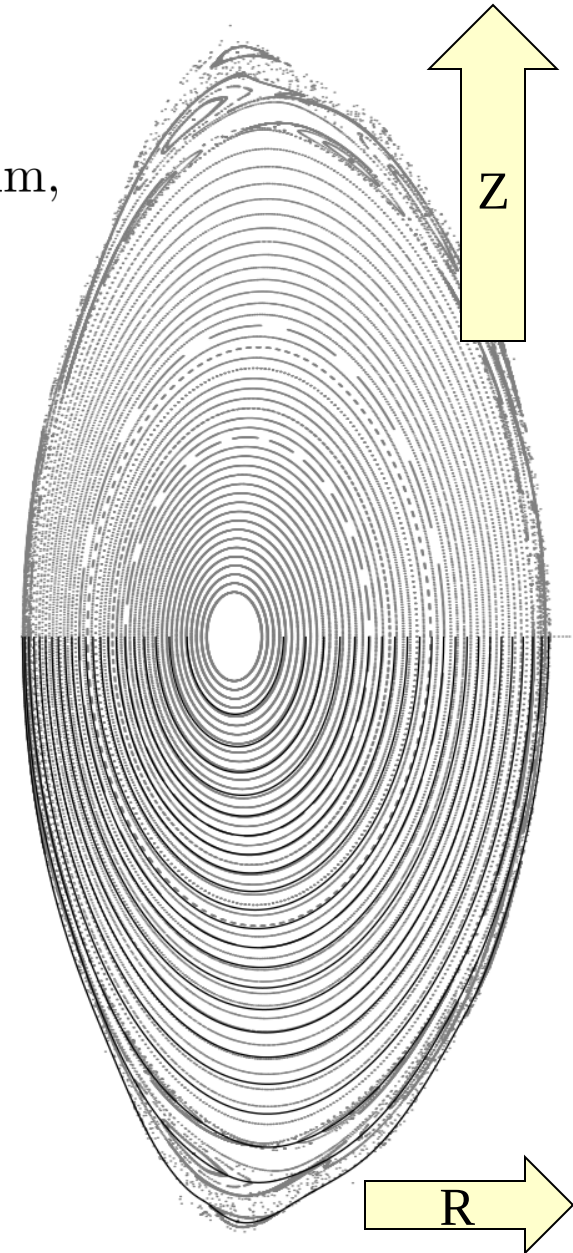

The corresponding islands lie on a coordinate surface

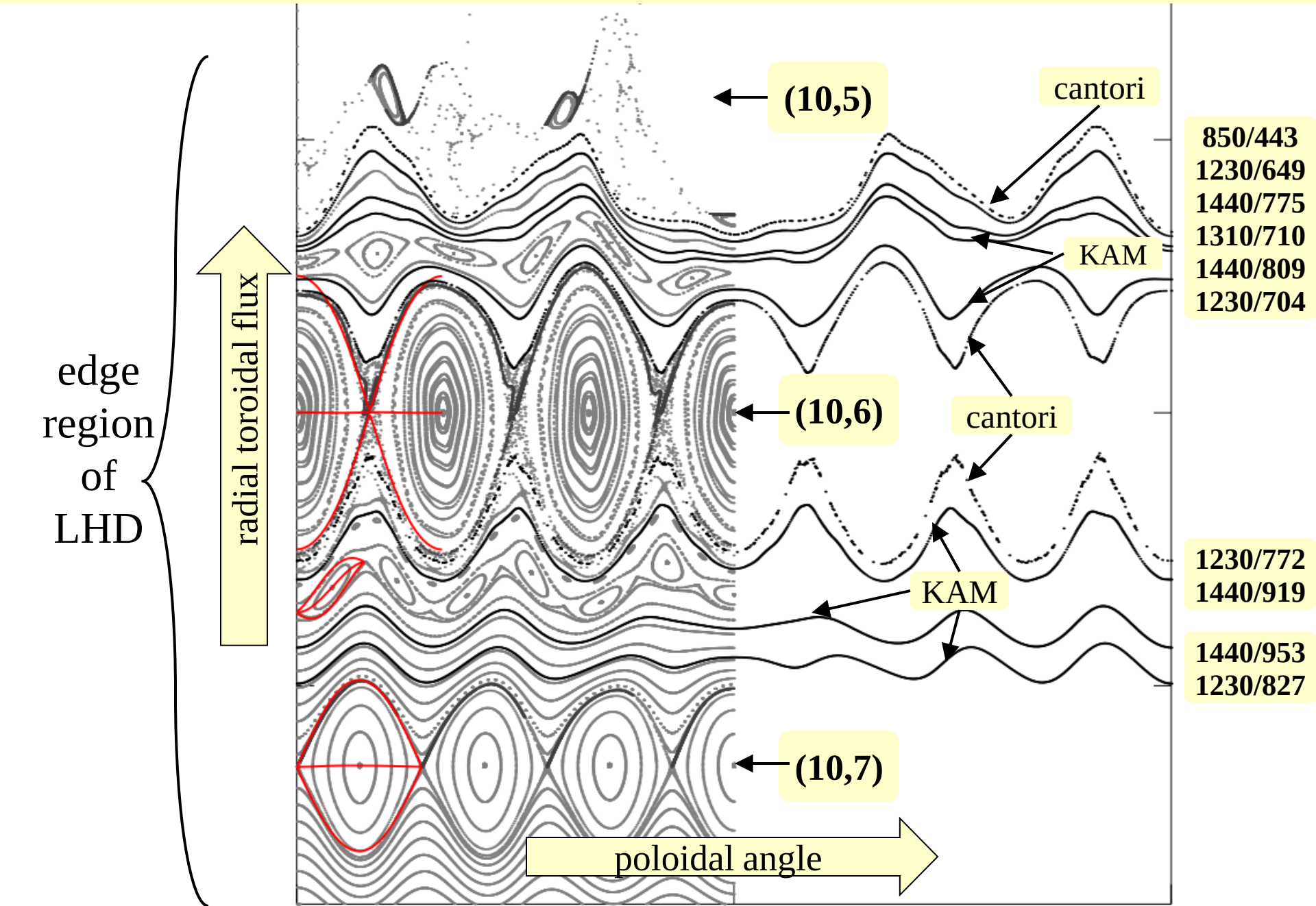

The Flux Farey tree shows the flux across the rational surfaces, the importance of the hierarchy of partial barriers can be quantified

1. $\oint_{\partial\mathcal{V}} \mathbf{B}\cdot d\mathbf{S} = \int_{\mathcal{V}} \nabla\cdot\mathbf{B}\, dv = 0$; the total flux across any closed surface is zero.

2. Consider any "ribbon" surface with boundary coinciding with X and O fieldlines; define "upward" flux
$$\Psi_{p/q} \equiv \oint_{\mathcal{S}} \mathbf{B}\cdot d\mathbf{S} = \int_O \mathbf{A}\cdot d\mathbf{l} - \int_X \mathbf{A}\cdot d\mathbf{l}.$$

3. Surfaces with small flux are "partial" barriers.

4. If $\Phi_{p/q}$ is suff. small, collisional transport can dominate.

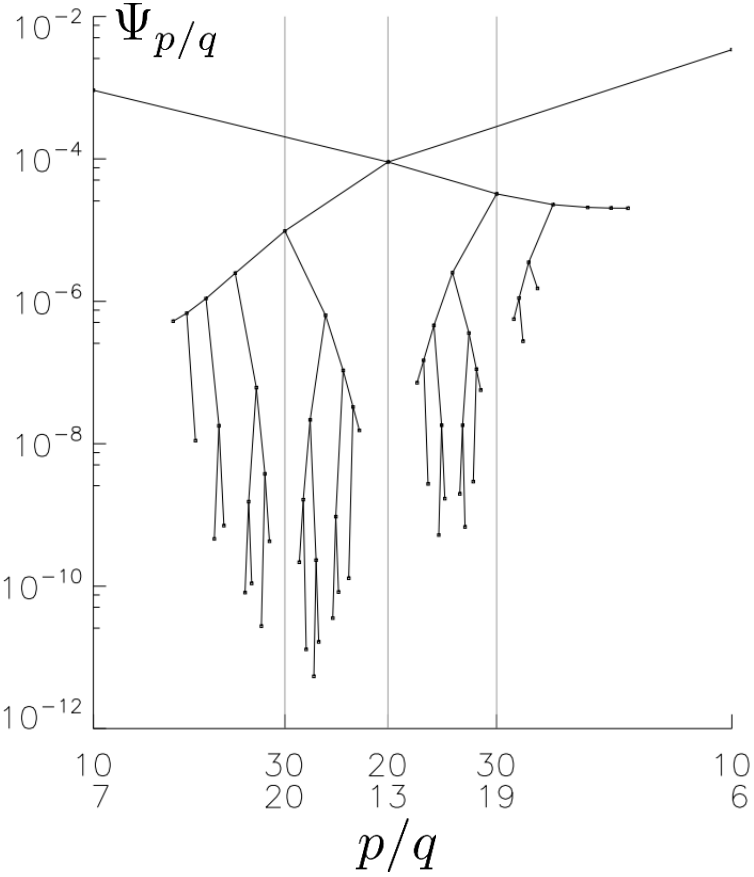

Now, construct more ghost surfaces

(resolve the fractal structure iteratively)

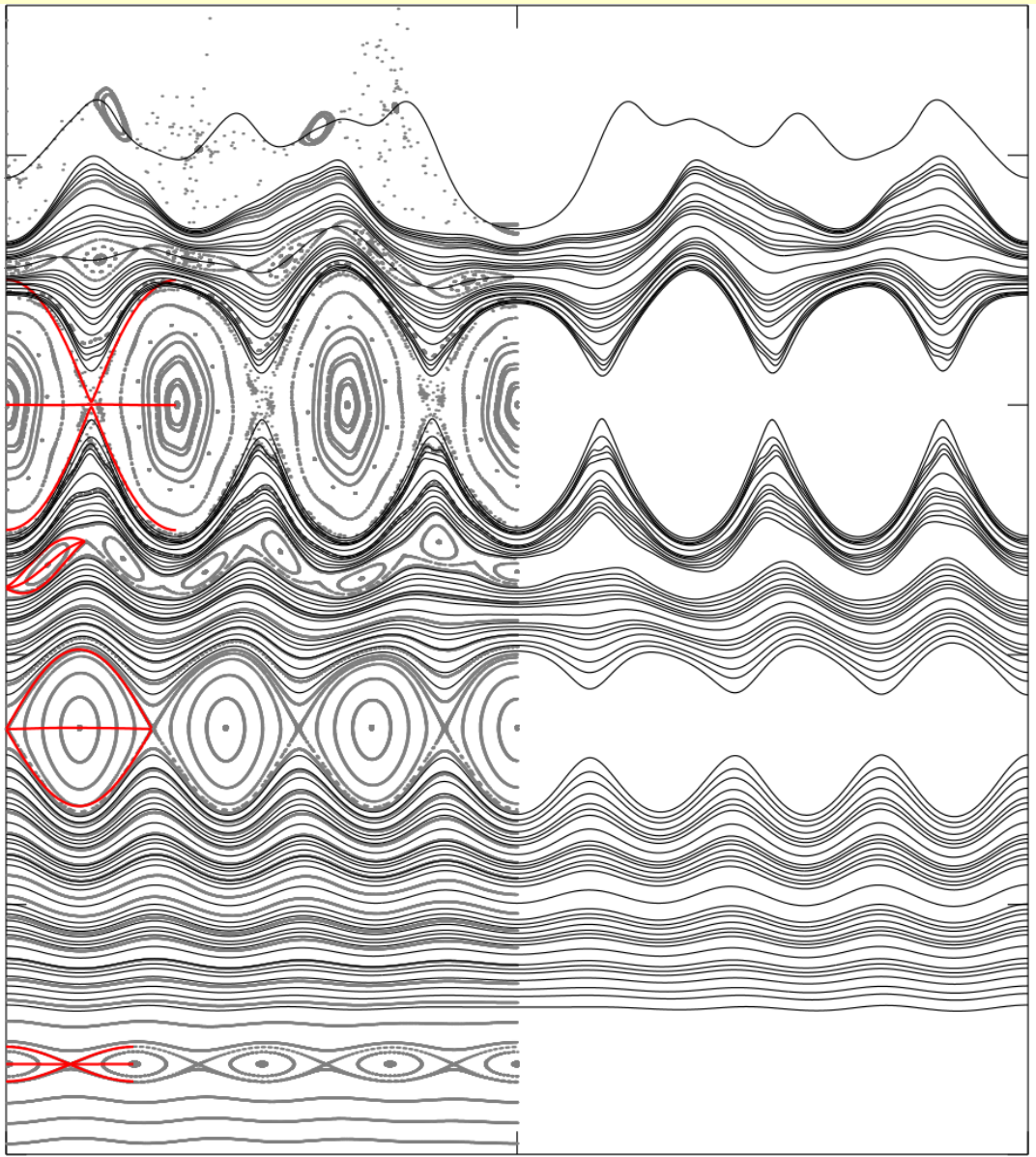

Poincaré plot.

Assuming no source in islands,
$T \approx T(\rho)$,
$p \approx p(\rho)$.

Numerical Solution to anisotropic transport

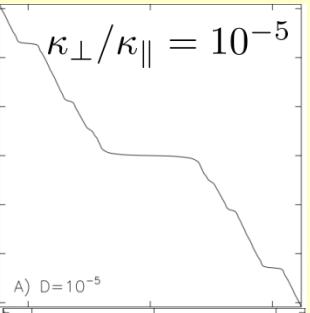

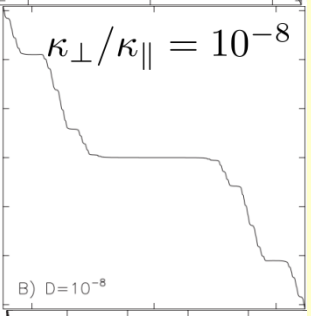

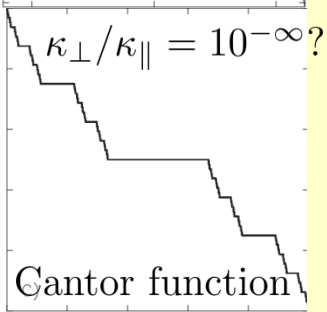

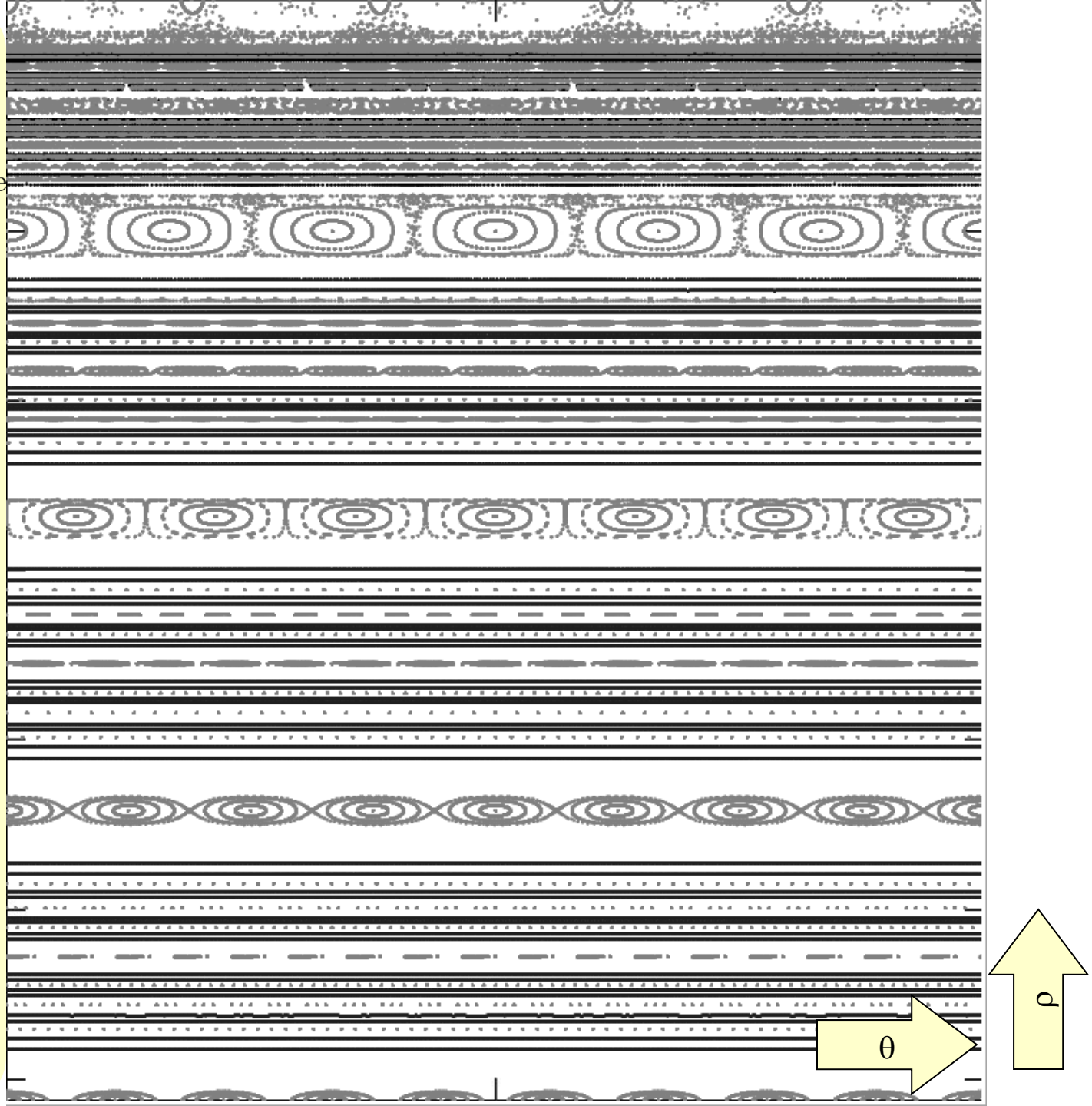

$\left(\frac{10}{5}\right)$
$\left(\frac{20}{11}\right)$
$\left(\frac{10}{6}\right)$
$\left(\frac{10}{7}\right)$
$\left(\frac{10}{8}\right)$
$\left(\frac{10}{9}\right)$

Poincaré plot.

Coordinates constructed by interpolation between QFM surfaces;

flux surfaces are straight.

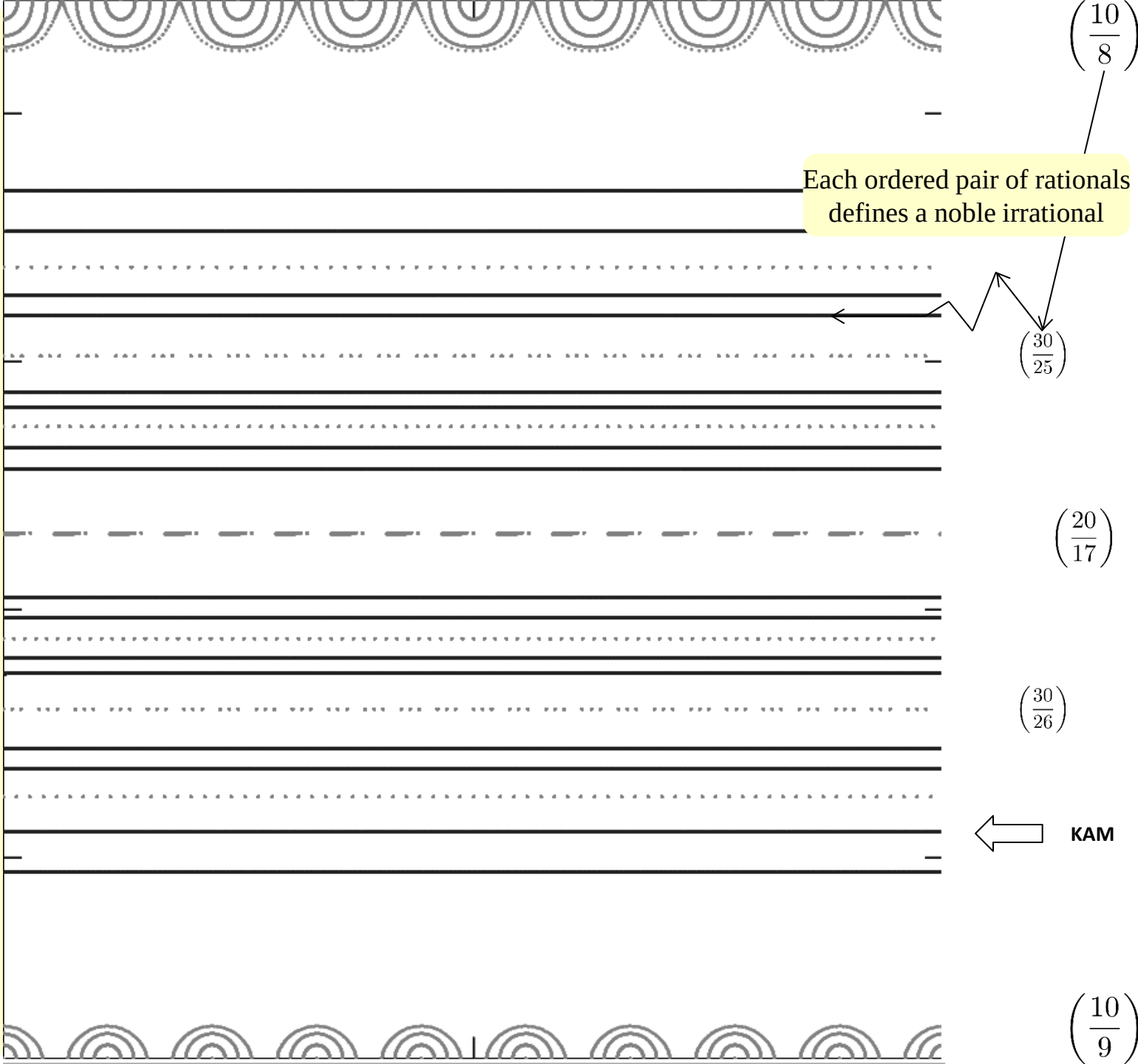

Poincaré plot.

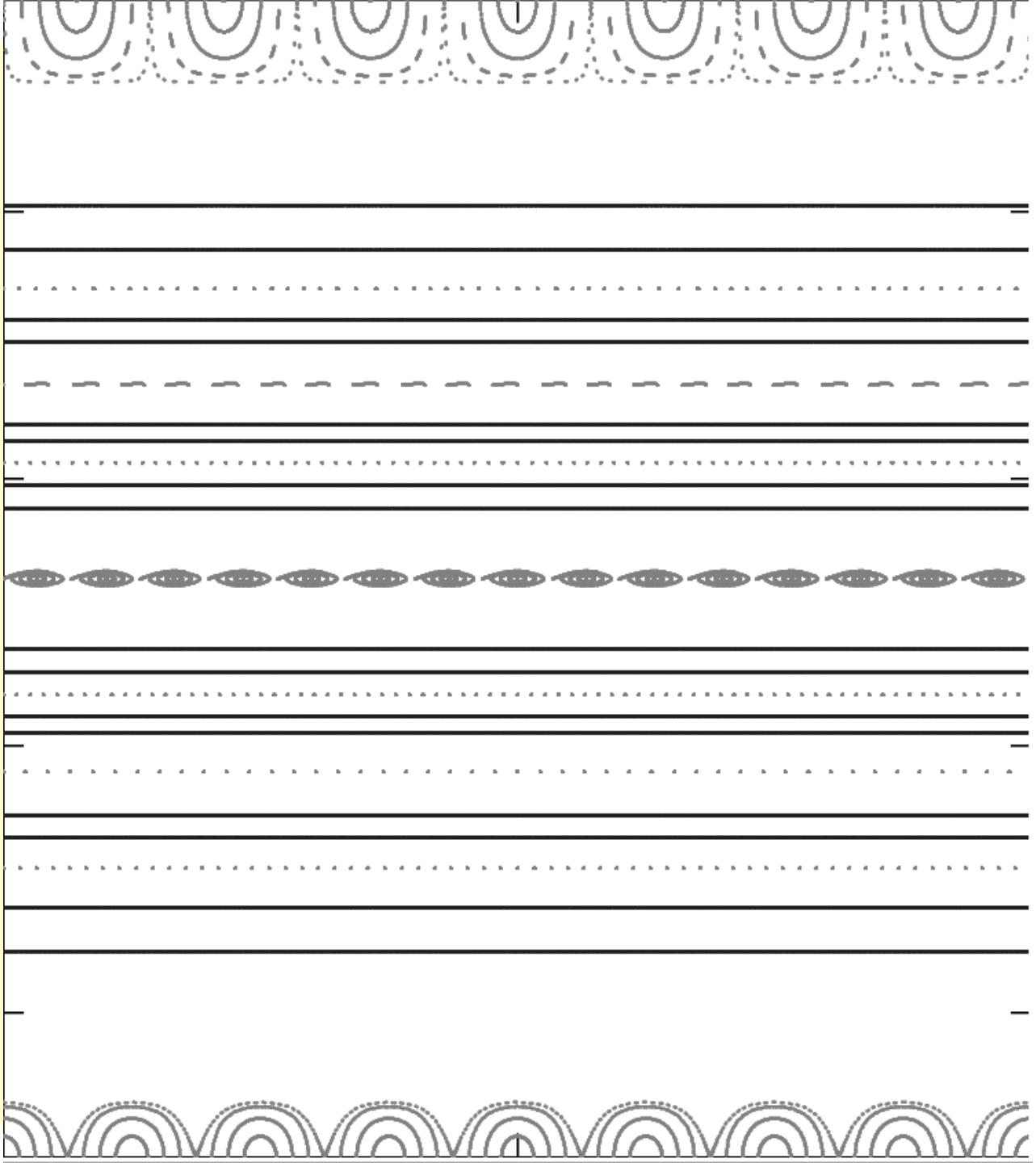

Poincaré plot.

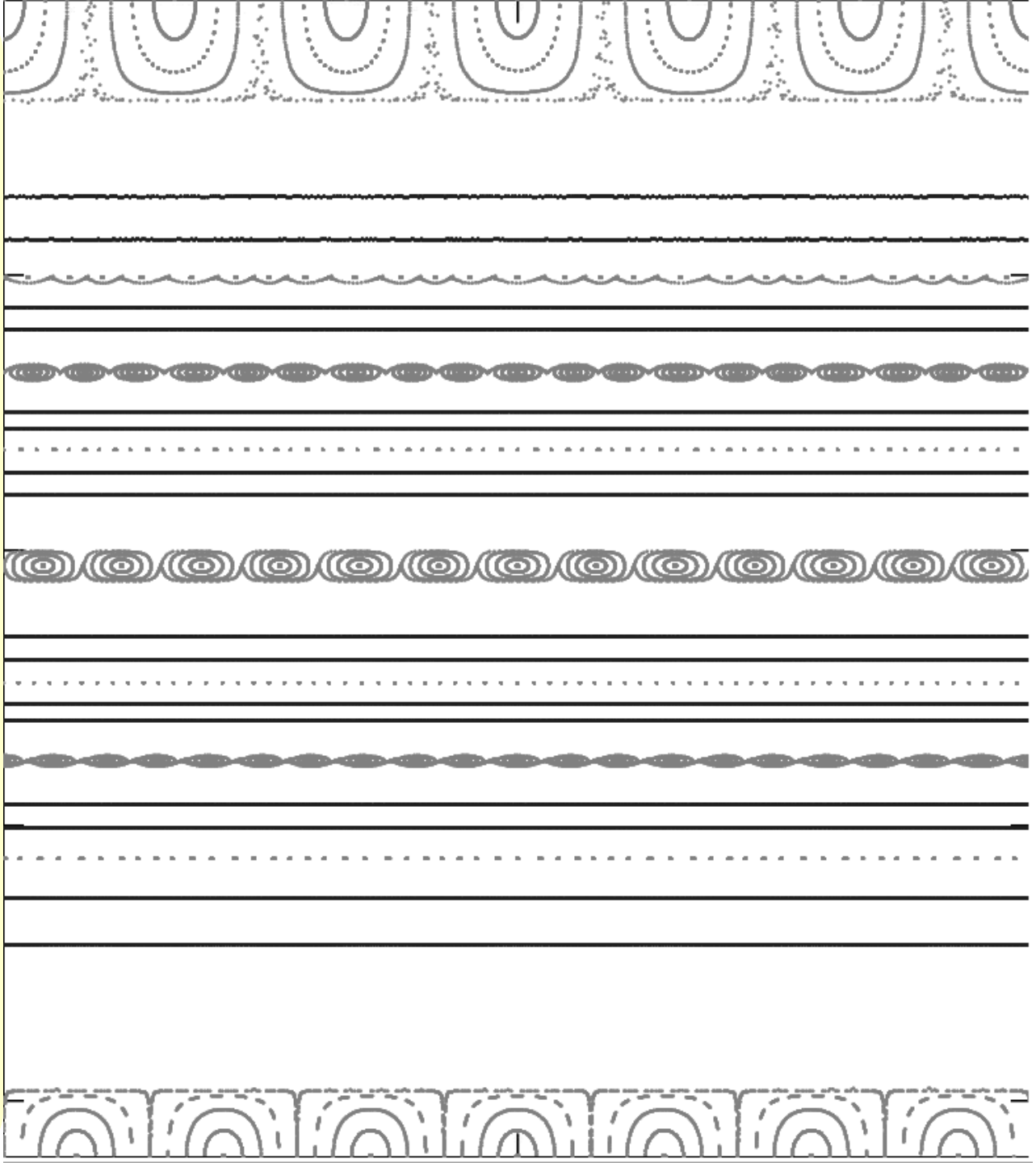

Islands become square.

Poincaré plot.

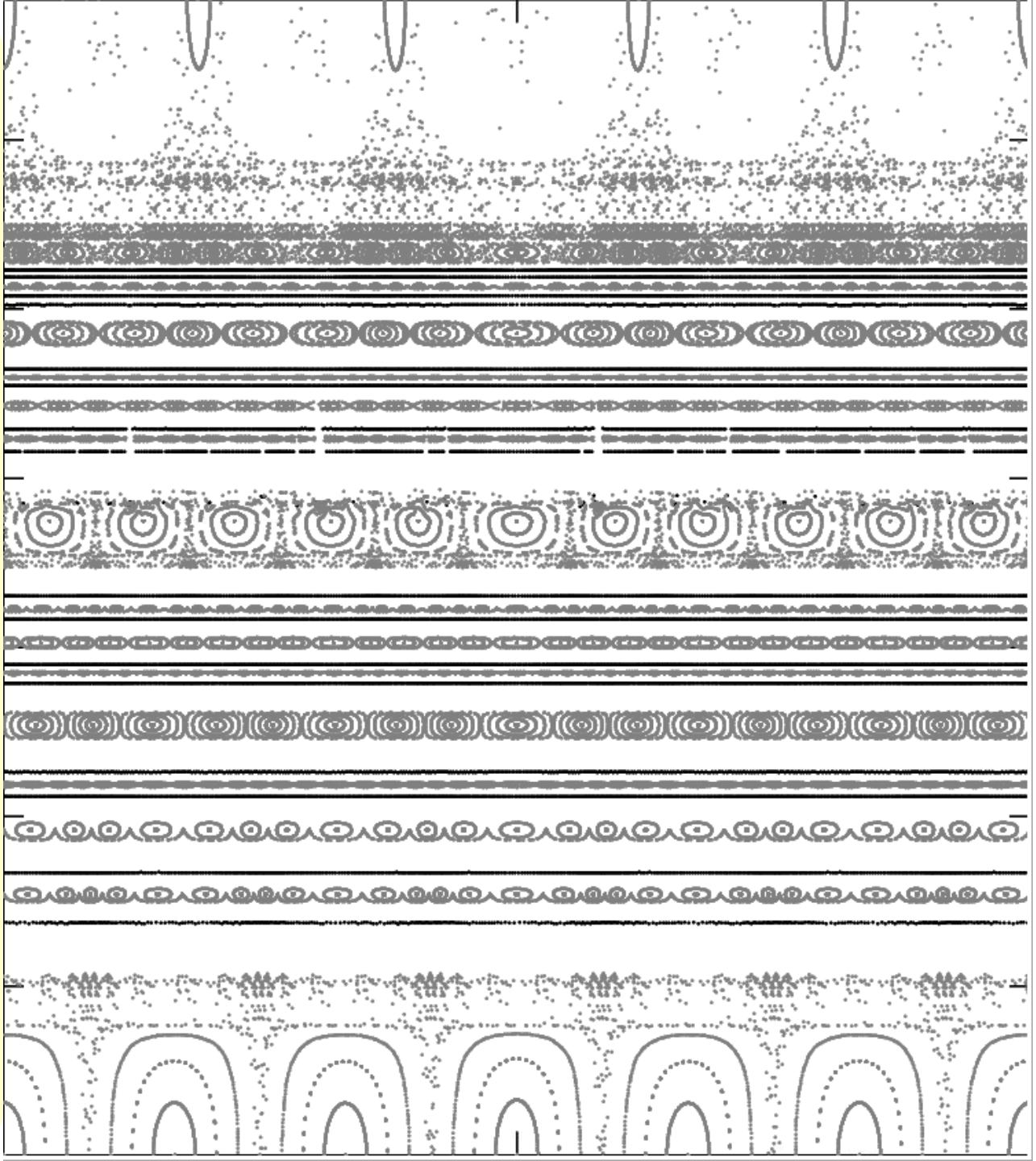

$\left(\frac{10}{5}\right)$

$\left(\frac{40}{21}\right)$

$\left(\frac{30}{16}\right)$

$\left(\frac{50}{27}\right)$

$\left(\frac{20}{11}\right)$

$\left(\frac{50}{28}\right)$

$\left(\frac{30}{17}\right)$

$\left(\frac{40}{23}\right)$

$\left(\frac{10}{6}\right)$

Poincaré plot.

Edge of confinement region is not a single, sharp barrier;

but instead a hierarchy of

i. islands,
ii. KAM, and
iii. cantori.

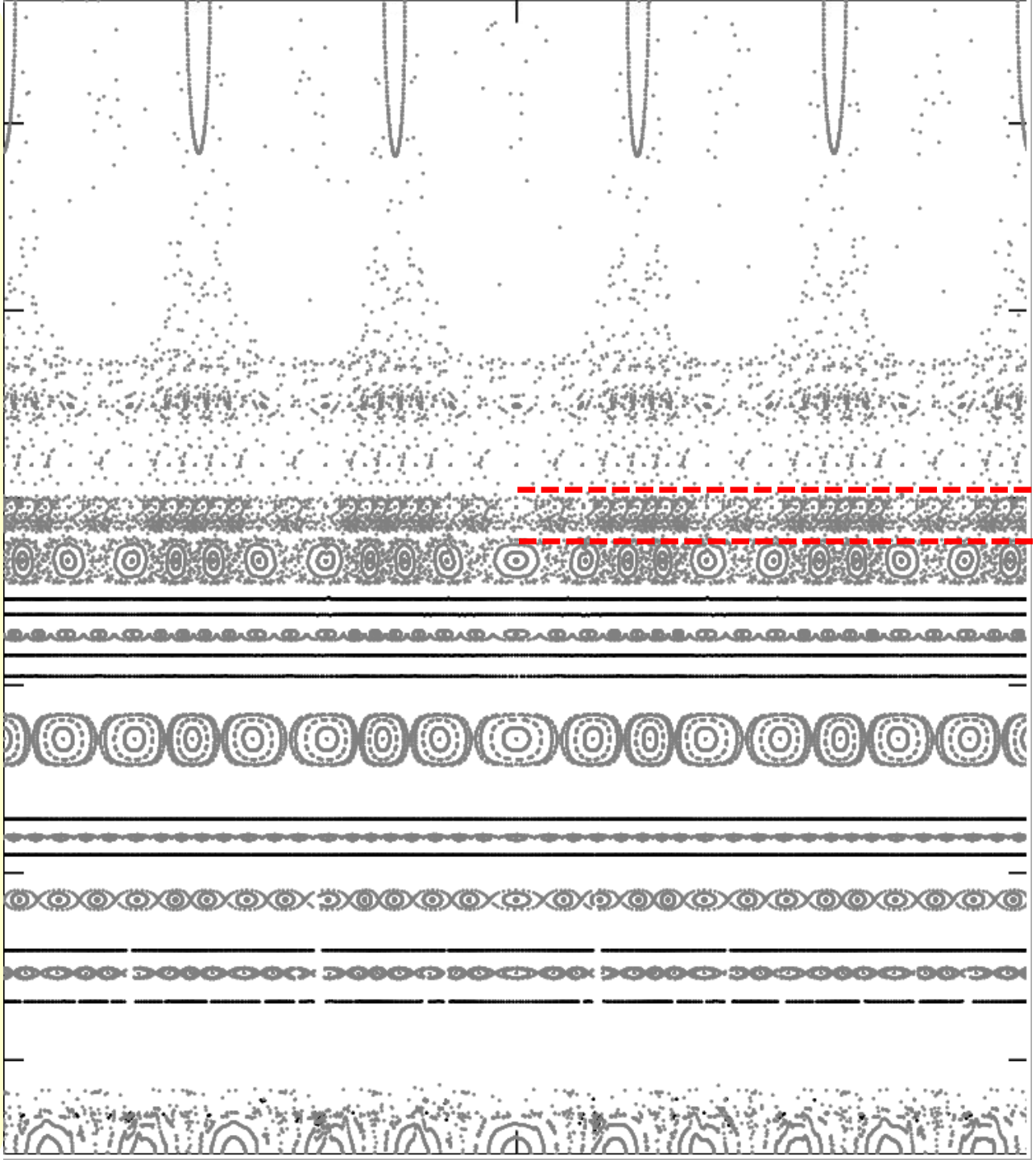

Anisotropic Heat Transport

Consider heat transport:
rapid transport along the magnetic field,
slow transport across the magnetic field.

1. Imagine that transport along $\mathbf{B}$ is unrestricted
   e.g. parallel random walk with long steps $\approx$ collisional mean free path.

2. Transport across the magnetic field is very small:
   e.g. perpendicular random walk with short steps $\approx$ Larmor radius.

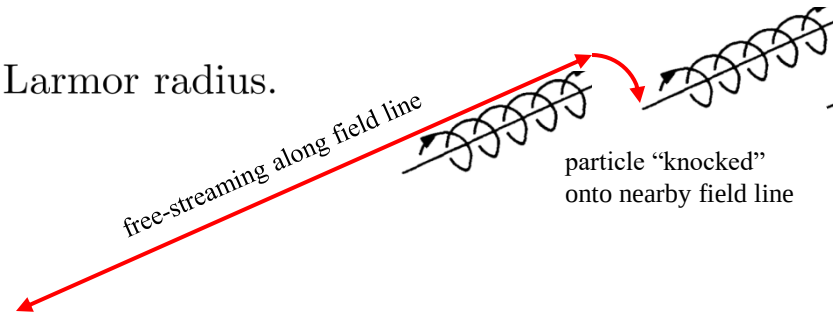

3. Simplest transport model: anisotropic diffusion,

$$\boxed{\frac{\partial T}{\partial t} = \nabla \cdot \left(\kappa_{\parallel} \nabla_{\parallel} T + \kappa_{\perp} \nabla_{\perp} T\right) + S}, \quad \kappa_{\perp}/\kappa_{\parallel} \sim 10^{-10},\ T \equiv \text{temperature};\ S \equiv \text{source};$$

4. Extreme anisotropy presents numerical challenges
   $\rightarrow$ extreme numerical resolution is required.

5. For computational efficiency, introduce "local fieldline coordinates".

   Construct coordinates (α, β, ζ) s.t. $\mathbf{B} \equiv \nabla\alpha \times \nabla\beta$, by local fieldline tracing;

   Parallel and perpendicular directions are treated separately, $\mathbf{B} \cdot \nabla \equiv B^{\phi}\partial_{\zeta}$, which reduces numerical diffusion.

   The parallel diffusion operator becomes $\nabla_{\parallel}^2 T = B^{\phi} \dfrac{\partial}{\partial \zeta}\left(\dfrac{B^{\phi}}{B^2}\dfrac{\partial T}{\partial \zeta}\right)$.

Numerical solution of anisotropic heat transport exploits field-aligned coordinates

1. Heat flux $\nabla \cdot \mathbf{q} = 0$, where $\mathbf{q} = \mathbf{b} \cdot \nabla T \, \kappa_{\|} \, \mathbf{b} + \kappa_{\perp} \nabla_{\perp} T$, strongly anisotropic.
2. Parallel relaxation employs field-alligned coordinates, $\mathbf{B} = \nabla\alpha \times \nabla\beta$, so parallel derivative is accurate, $\nabla^2_{\|} T = \dfrac{\partial^2 T}{\partial \eta^2} = B^{\zeta} \dfrac{\partial}{\partial \zeta} \left(\dfrac{B^{\zeta}}{B^2} \dfrac{\partial T}{\partial \zeta} \right)$.
3. Perpendicular relaxation simply $\nabla^2_{\perp} T = \dfrac{\partial^2 T}{\partial \alpha^2} + \dfrac{\partial^2 T}{\partial \beta^2}$.
4. Sparse linear system solved iteratively on numerical grid, resolution $= 2^{12} \times 2^{12}$.

Poincaré plot

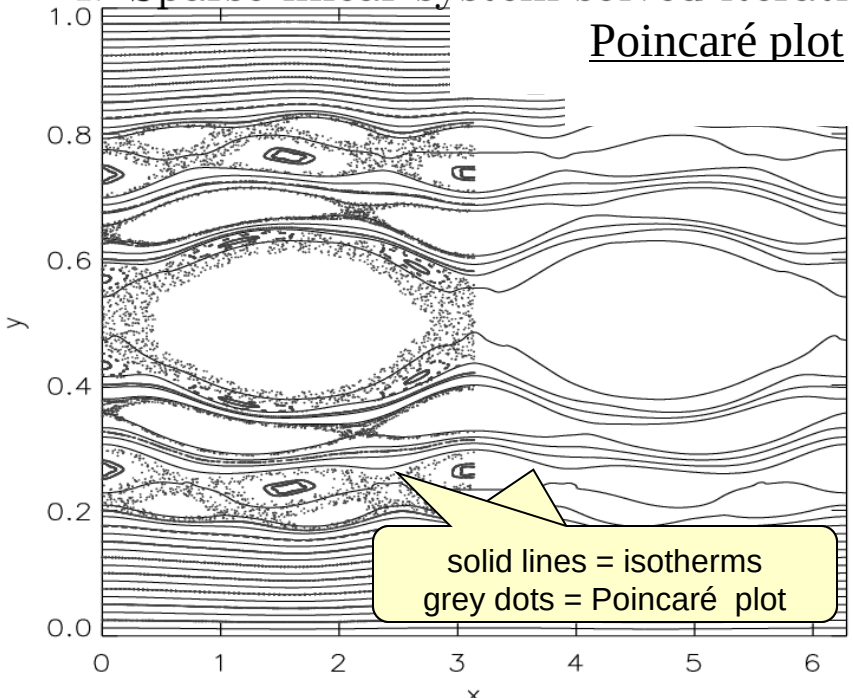

Error vs grid resolution

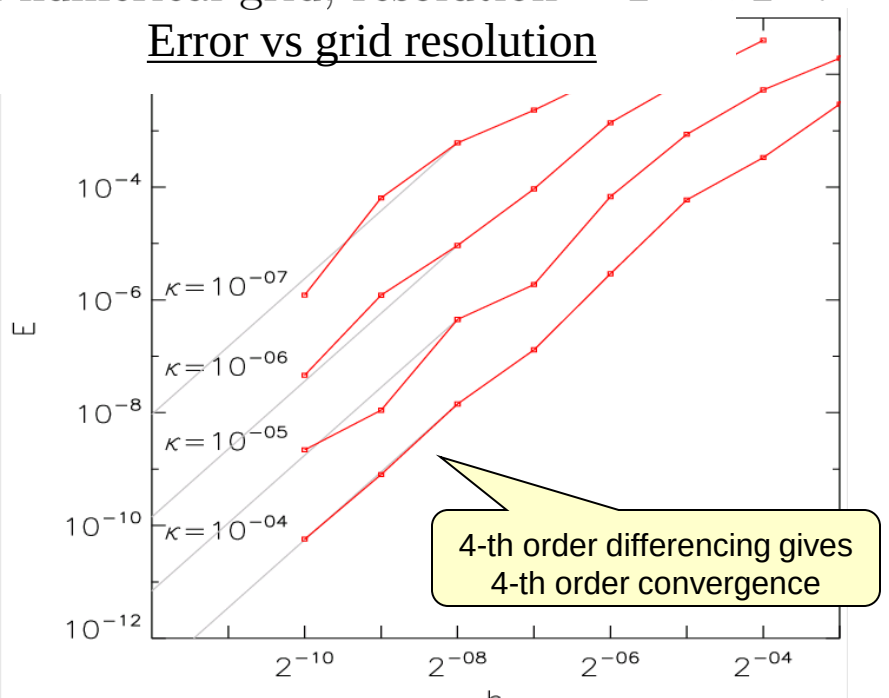

Isotherms of the steady state solution to the anisotropic diffusion coincide with ghost surfaces; analytic, 1-D solution is possible.

1. The temperature is constant on KAM surfaces, cantori, and ghost-surfaces, i.e. $T = T(\rho)$.

2. From $T = T(\rho, \theta, \zeta)$ to $T = T(\rho)$ allows

$$\boxed{\frac{dT}{d\rho} \propto \frac{1}{\kappa_{\|}\varphi_2 + \kappa_{\perp} G}},$$

where

$$\varphi_2 \equiv \underbrace{\int B_n^2 \, d\mathbf{s}}_{\text{quadratic flux}}, \quad \text{and}$$

$$G \equiv \underbrace{\int \nabla\rho \cdot \nabla\rho \, d\mathbf{s}}_{\text{metric}}.$$

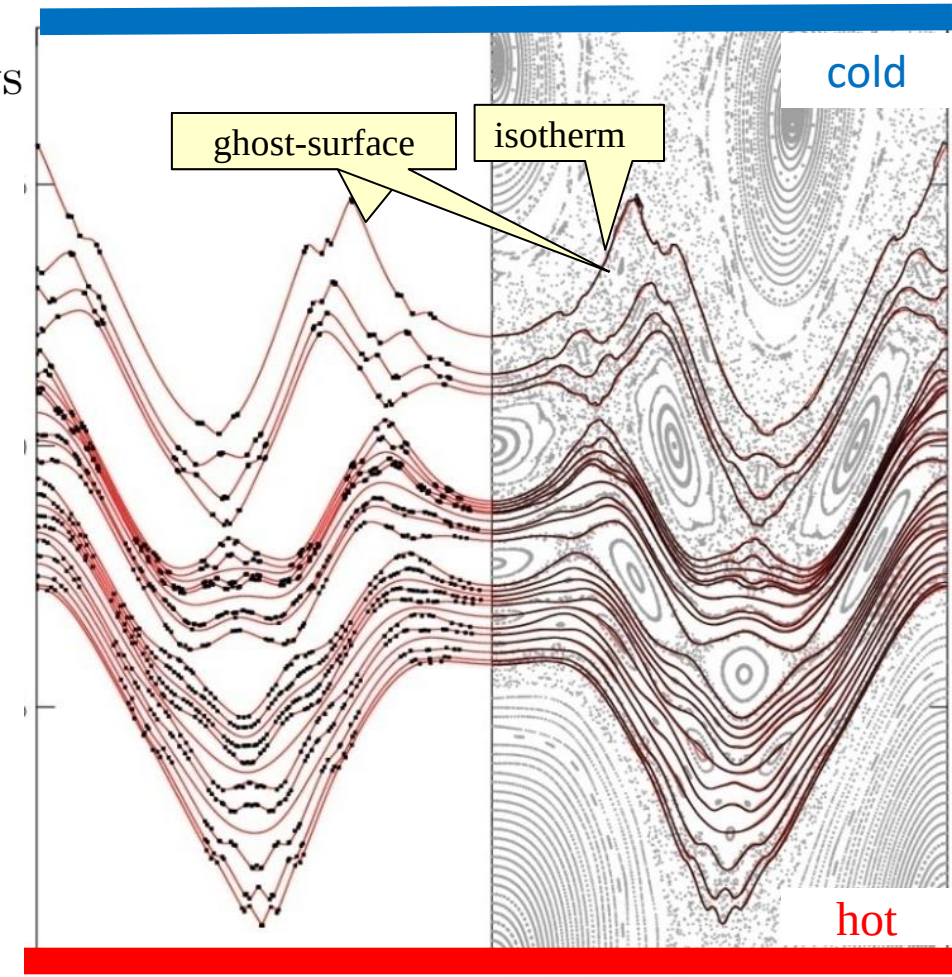

Chaotic coordinates simplify temperature profile to a smoothed Diophantine (fractal) staircase

1. From $0 = \dfrac{\partial}{\partial s}\displaystyle\int_V \nabla\cdot\mathbf{q}\,dv = \dfrac{\partial}{\partial s}\int_{\partial\mathcal{V}} \mathbf{q}\cdot\mathbf{n}\,d\sigma$, assume $T = T(s)$ to derive $T' = \dfrac{const.}{\kappa_\parallel \Omega + \kappa_\perp G}$

   for quadratic-flux $\Omega = \displaystyle\int g^{ss}\frac{B_n^2}{B^2}\,d\sigma$, and metric $G = \int g^{ss} d\sigma$, $g^{ss} = \nabla s\cdot\nabla s$.

2. In the "ideal limit", $\kappa_\perp \to 0$, $T'(s) \to \infty$ on irrational KAM surfaces (where $\Omega = 0$).

3. Non-zero $\kappa_\perp$ ensures $T(s)$ is smooth; $T'(s)$ peaks on minimal Ω surfaces = noble cantori.

Temperature Profile

$$\frac{\kappa_\parallel}{\kappa_\perp} = 10^{10}$$

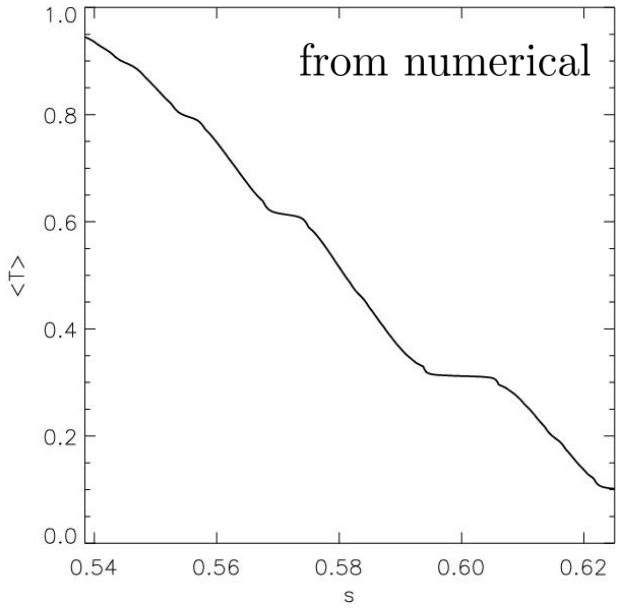

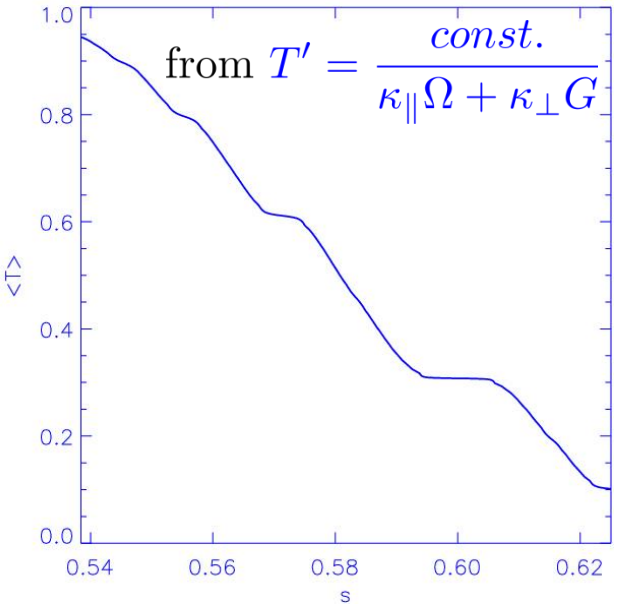

Comments

1. The "geometry" of integrable dynamics can be incorporated into the coordinates

   action-angle coordinates.

2. The geometry and "fractal-ness" of non-integrable dynamics
   can be incorporated into the coordinates

   "chaotic coordinates".

3. In the limit that all the regular dynamics is incorporated,
   the coordinates become pathological.

4. In practice, some "smoothing" diffusion-type effects

Unstable manifold

The magnetic axis is a "stable" fixed point (usually), and the X-point is "unstable". Consider the eigenvalues of tangent mapping:

1. Consider following a fieldline nearby a fixed point, $\mathbf{x}_0 + \delta\mathbf{x}$, around many toroidal periods:

$$\underbrace{\nabla\mathbf{M} \cdot \ldots \nabla\mathbf{M}}_{\text{tangent mapping}} \cdot \delta\mathbf{x} = (\nabla\mathbf{M})^n \cdot \delta\mathbf{x} = (\nabla\mathbf{M})^n \cdot \underbrace{(a\,\mathbf{v}_u + b\,\mathbf{v}_s)}_{\text{eigenvectors}} = a\,\lambda_u^n\,\mathbf{v}_u + b\,\lambda_s^n\,\mathbf{v}_s$$

2. The determinant, $|\nabla\mathbf{M}| = 1$ at fixed points (because $\nabla \cdot \mathbf{B} = 0$), so the eigenvalues are either:

i. complex congugates, $\lambda = \alpha + \beta\,i$, $\lambda = \alpha - \beta\,i$, and the fixed point is stable:
nearby trajectories rotate: rotational-transform on axis, $\tan\iota = \beta/\alpha$.

ii. real reciprocals, $\lambda_u > 1$ and $\lambda_s = 1/\lambda_u$, and the fixed point is unstable:
nearby trajectories diverge: $\lambda_u^n \to \infty$ as $n \to \infty$, $\lambda_s^n \to 0$ as $n \to \infty$;
$\mathbf{v}_u$ indicates unstable direction, $\mathbf{v}_s$ indicates stable direction.

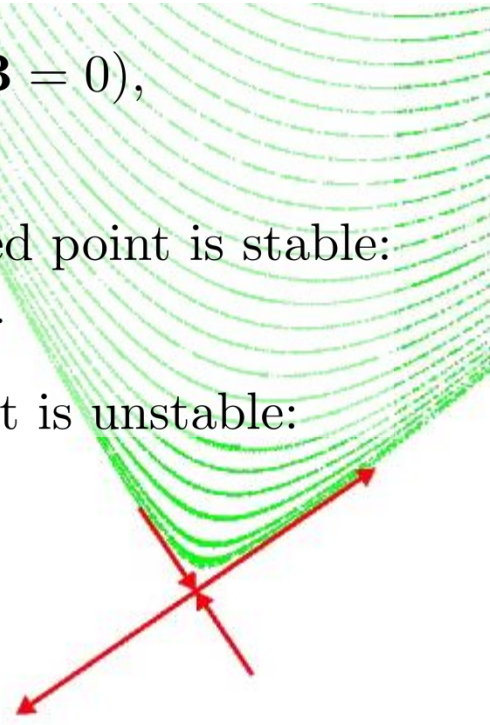

The stable/unstable direction forwards in ϕ is the unstable/stable direction backwards in ϕ.

1. $\mathbf{x} \in$ " stable manifold " if $\mathbf{M}^n(\mathbf{x}) \to \mathbf{x}_0$ as $n \to +\infty$.

   all magnetic fieldlines with "starting point" $\mathbf{x} = \mathbf{x}_0 + d\,\mathbf{v}_s$, where $d \in [\epsilon\lambda_s, \epsilon]$, and follow *backwards* in ϕ.

2. $\mathbf{x} \in$ "unstable manifold" if $\mathbf{M}^n(\mathbf{x}) \to \mathbf{x}_0$ as $n \to -\infty$.

   all magnetic fieldlines with "starting point" $\mathbf{x} = \mathbf{x}_0 + d\,\mathbf{v}_u$, where $d \in [\epsilon/\lambda_u, \epsilon]$, and follow *forwards* in ϕ.

3. For the integrable case, the unstable manifold leads into the stable manifold, and there is a "clean" separatrix.

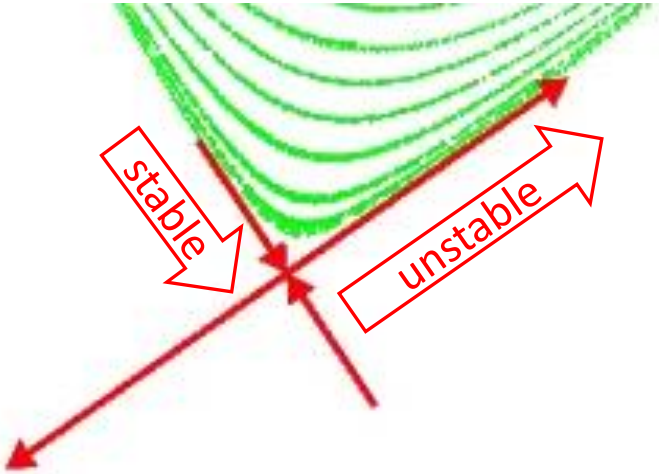

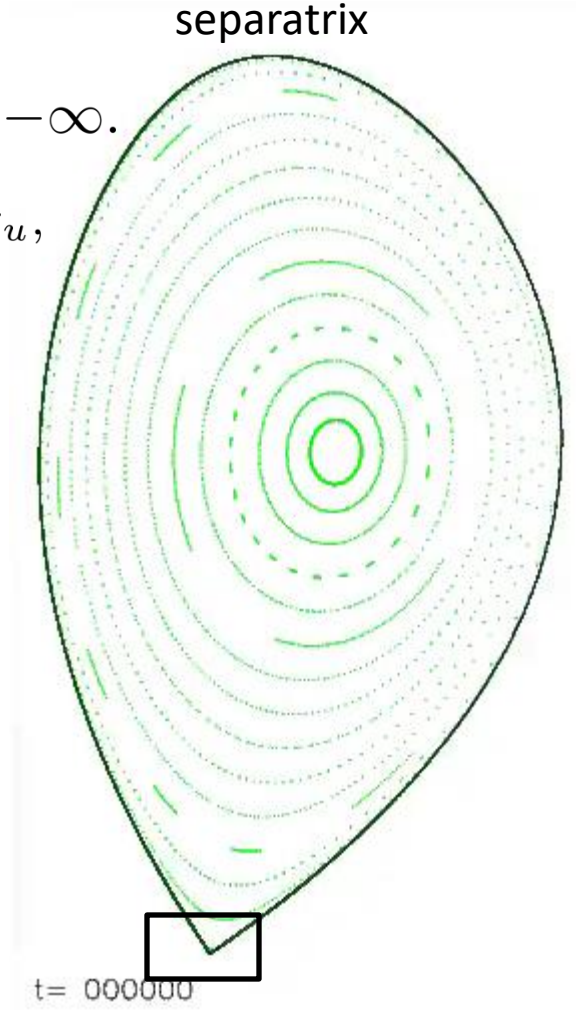

For perturbed magnetic fields, the separatrix splits. A "partial" separatrix can be constructed.

1. "Homoclinic" points, $\mathbf{x}_h \equiv$ intersection of stable, unstable manifolds, $\mathbf{M}^n(\mathbf{x}_h) \to \mathbf{x}_0$ as $n \to \pm\infty$.

2. To locate $\mathbf{x}_h$, find (d_u, d_s), $\mathbf{M}^{+i}(\mathbf{x}_0 + d_u\,\mathbf{v}_u) = \mathbf{M}^{-j}(\mathbf{x}_0 + d_s\,\mathbf{v}_s)$,

   if $\mathbf{x}_h$ is homoclinic, so is $\mathbf{M}^k(\mathbf{x}_h), \forall k$.

3. Partial separatrix
   = "smooth" part of unstable manifold
   + "smooth" part of stable manifold.

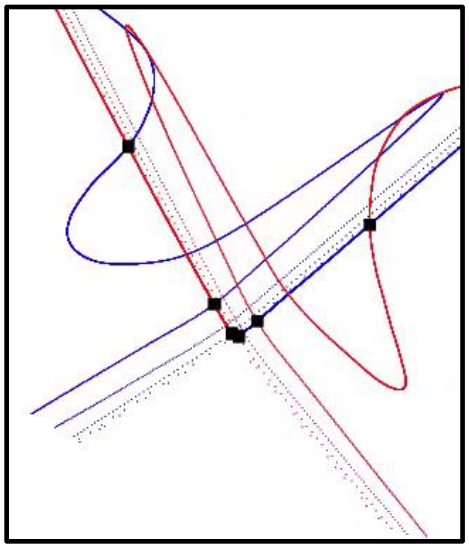

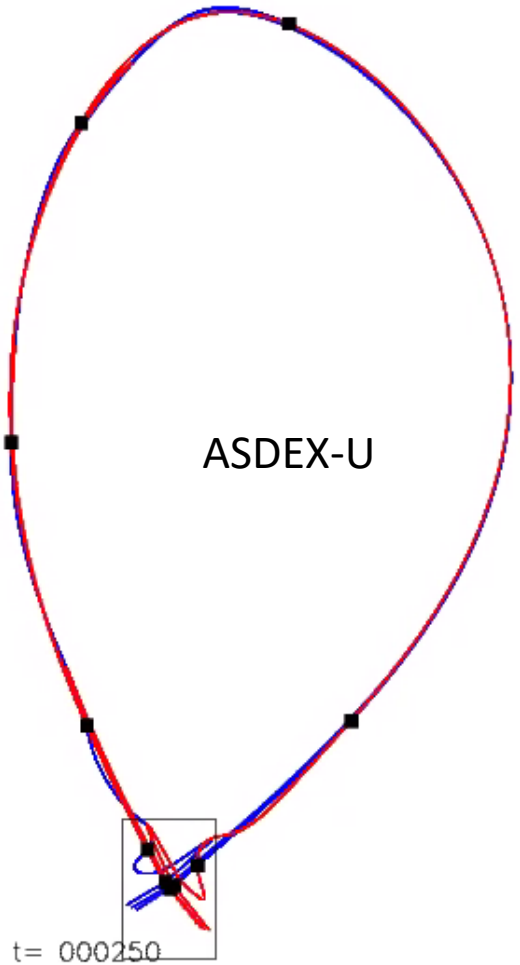

Anisotropic heat transport + unstable manifold = ?

What is the temperature in the “chaotic edge” ?

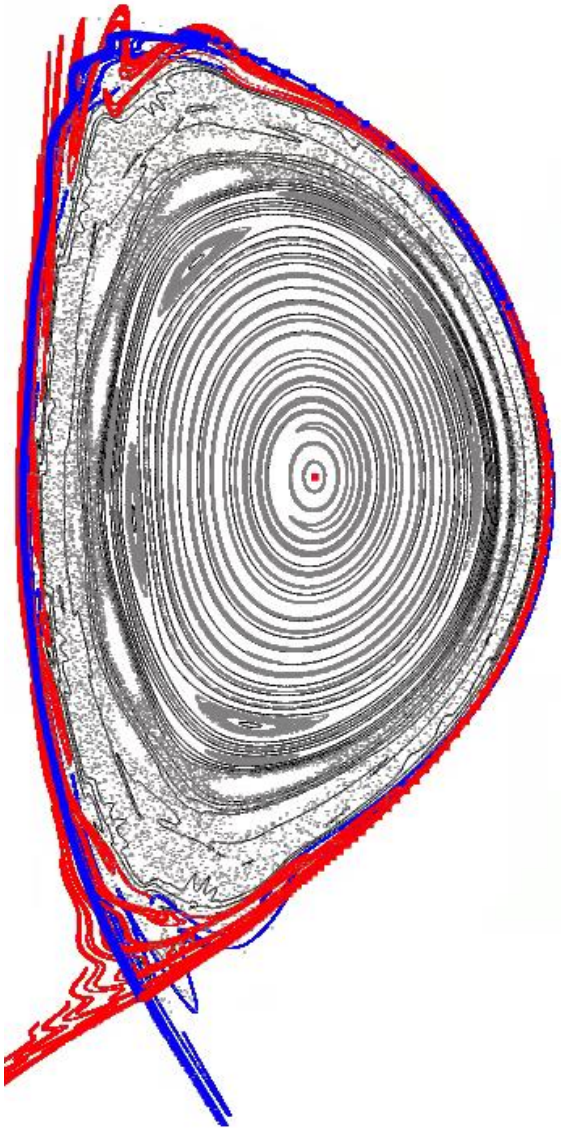

Anisotropic heat transport + unstable manifold = ?

What is the temperature in the “chaotic edge” ?